Author/s:
Li, S;Tsang, HH;Lam, N

Title:
Seismic protection by rocking with superelastic tendon restraint

Date:
2022-06-01

Citation:
Li, S., Tsang, H. H. & Lam, N. (2022). Seismic protection by rocking with superelastic tendon restraint. Earthquake Engineering and Structural Dynamics, 51 (7), pp.1718-1737. https://doi.org/10.1002/eqe.3635.

Persistent Link:
https://hdl.handle.net/11343/308213

Received: 30 December 2021 | Revised: 24 February 2022 | Accepted: 26 February 2022

DOI: 10.1002/eqe.3635

WILEY

RESEARCH ARTICLE

# Seismic protection by rocking with superelastic tendon restraint

**Sheng Li**[1] | **Hing-Ho Tsang**[2] | **Nelson Lam**[1]

[1]Department of Infrastructure Engineering, The University of Melbourne, Melbourne, Australia

[2]School of Engineering, Swinburne University of Technology, Melbourne, Australia

**Correspondence**
Sheng Li, Department of Infrastructure Engineering, The University of Melbourne, Melbourne, Australia.
Email: shengl1@student.unimelb.edu.au

**Abstract**

This article introduces an innovative system for enhancing the seismic performance of a structure through facilitating large rotational (rocking) motion to occur without risking overturning. The innovation of this study is in the use of tendons consisting of Nickel-Titanium (superelastic) alloy connected in series with steel to impose partial restraints to the structure when experiencing rocking motion. Importantly, the large rotational motion is fully recoverable. Existing installations which can be made to rock may also be retrofitted with the device for improving its seismic resistance. The original contributions of the article are the derivation, and experimental validation, of an analytical model for simulating the seismic performance of a system that has been fitted with the restraining device. In a parametric study employing the newly developed modelling techniques, major trends in the seismic response behaviour of the structure have been identified.

**KEYWORDS**

seismic protection, rocking, superelastic tendon, dynamic test, displacement

## 1 | INTRODUCTION

The conventional approach of achieving high seismic performance of a structure is to enhance its capacity to displace well beyond the yield limit whilst maintaining adequate lateral resistance. As the structure experiences a substantial amount of post-elastic deformation, much of the kinetic energy of the structure can be dissipated. Through ductile design and detailing, the structure is made capable of developing a robust deformation mechanism to fulfil the stated performance objectives. However, significant damage to the structure can occur, and the deformation can be largely unrecoverable (Figure 1A). The main drawbacks with the approach of making use of ductility to absorb energy are the loss of the continuous functionality of the built facility and the costly repair required to reinstate the structure for reoccupation. Worse still, the structure may have to be written off completely.

An alternative approach of achieving high seismic performance of a structure is to allow the vertical supporting element, such as a structural wall[1–4] or a bridge pier,[5–7] to experience large whole-body rotation about the base. This type of motion, which is herein referred to as rocking motion, makes use of the lifting of the centre of gravity of the structure, or part of the structure, to dissipate large amounts of energy. As rocking is facilitated, the need to absorb energy through the straining of materials can be circumvented. Furthermore, rocking also elongates the natural period of vibration of the structure, which reduces the amount of energy transferring from the base to the superstructure. The idea of enhancing the seismic

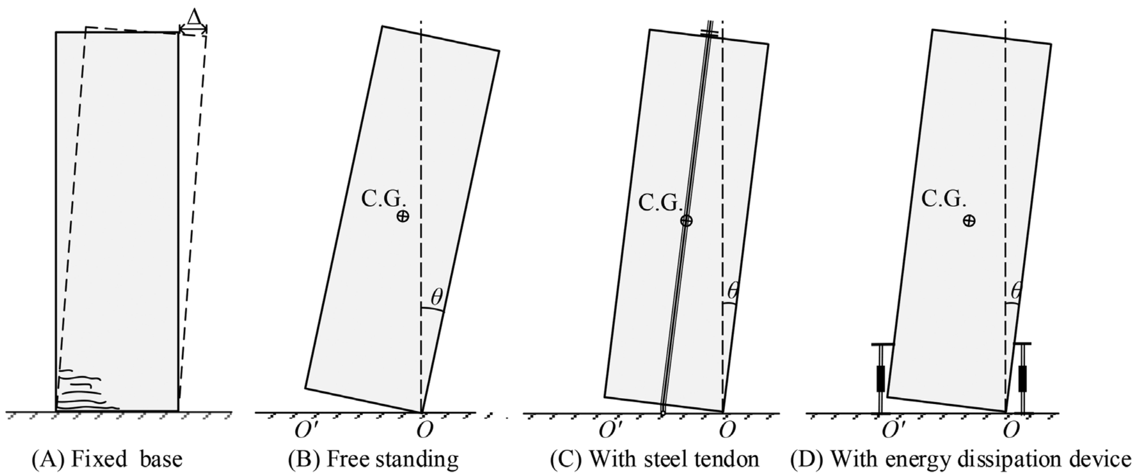


**FIGURE 1** Seismic performance enhancement for a rocking block with supplementary devices

performance of a structure by developing a viable rocking mechanism has been around for a long time.[8–10] This concept is illustrated in the schematic diagram of Figure 1B.

The risk of overturning can increase rapidly with increasing the angle of rotation. Allowing this angle to come close to the limit of overturning can prolong the tilting of the structure, and hence introduce considerable uncertainties into the outcome of the rocking response.[11,12] High rotation can also cause severe pounding of the structure at the base resulting in excessive damage. In a recent investigation on the seismic safety of a modular building (undertaken by the last author and colleagues), the overturning risk was found to be aggravated significantly by the brittle failure of the bolted connections immediately prior to the commencement of rocking.[13] Thus, a viable rocking mechanism for enhancing seismic performance has to be properly engineered to facilitate the desirable movement unhindered, and to have the extent of rotation kept under control. Non-structural components including utility ducting would also be required to accommodate the rocking motion.

For structural walls that have been designed to rock in an earthquake, the adjoining building frames can be relied upon to provide restraints to control the rotation. Bridge piers designed to rock can also derive support from the bridge deck, which is in turn connected to other bridge piers or the abutments. For a whole-body rocking structure, which is the subject of this study, there can be no such redundancies from which to derive support. Incorporating suitable restraints forming part of the designed rocking mechanism is therefore necessary.

Three kinds of restraining systems for controlling rocking have been proposed in the literature. The first kind is the use of vertical prestressing cables which extend the full height of the structure (Figure 1C). This approach to design has been investigated[14] and there are scopes of making improvements because of the need to keep the cable to deform within the elastic limit, given that the post-elastic elongation of steel is unrecoverable and the risk of fracture can be high. With this design option, the amount of rotation would be very limited. The second kind of control is the use of energy dissipation devices (Figure 1D), such as the base-plate-yielding rocking systems,[15] the replaceable reinforcing steel bars in short length,[16] the dampers[17–19] or the inerters.[20–24] The third kind is the combined use of the prestressing cables and energy dissipation devices, such as the combination of cables with the dampers,[25] the energy dissipation bars,[26] the steel sleeve,[27,28] or the O-shaped connectors.[29,30]

A structure which has been facilitated to experience large rotational motion as a whole body is referred herein as the 'rocking block'. This article aims at introducing the use of an alloy material that has the ability to reverse the response to applied stress in an elastic manner through phase transformation between the austenitic and martensitic phases of the crystals. This type of behaviour is known as 'superelastic' behaviour.[31–33] The use of the superelastic tendon is introduced in this article as an alternative approach of controlling the rocking motion of the block in conditions of intense ground shaking. A number of alloy systems exhibit superelasticity. The Nickel-Titanium (NiTi) alloy is widely used because of its high strength, high ductility, and excellent corrosion resistance,[33] and there is continuous development of the superelastic material for better temperature performance.[32,34] Because of its excellent deformation recovering rate and relatively stable hysteretic behaviour,[35] many researchers have used shape memory material or superelastic material for seismic enhancement purposes, such as the angle shape fixings,[36] the braces of frames,[37,38] or the bearings.[39,40] The original contribution of this article is in mitigating the seismic response of a rocking block through allowing it to experience controlled rocking

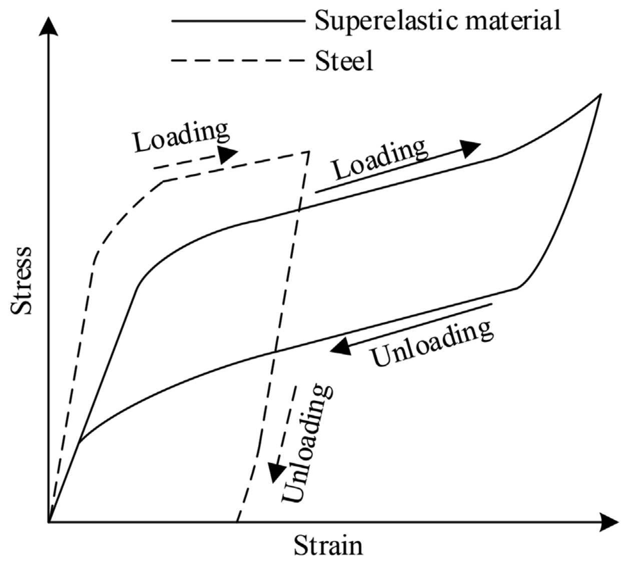


**FIGURE 2** Schematic strain-stress relationship of Nickel-Titanium (NiTi) alloy and high yield steel

as a whole body by the use of superelastic materials. This mitigating feature can be incorporated into the seismic design of structures such as modular buildings, slender tanks and similar installations.

The analytical models of free rocking structure and elastic tendon constrained rocking structure have been developed and validated by other researchers.[41–43] The analytical model of superelastic tendon constrained rocking structure, and experimental validations of the accuracy of the analysis will be presented in this paper to facilitate the design process as original contributions to knowledge.

The conception of the new prestressing systems is introduced next, which is followed by analytical modelling for simulating the time-history of the rocking motion (Section 2). To validate the analytical results, experimental tests have been undertaken to demonstrate agreement between the modelled and recorded results. Details of the validation will be presented as original contributions to knowledge (Sections 3 and 4). Results from dynamic physical testing, and numerical simulations, will be employed in case studies to demonstrate the viability of the proposed system in enhancing the seismic performance of prototype models and to reveal major trends in order that the potential response behaviour of the innovative system in projected earthquake scenarios can be made predictable (Section 5).

## 2 | CONCEPTUAL DEVELOPMENT AND ANALYTICAL MODELLING

### 2.1 | Conceptual development

A fundamental requirement of the proposed innovation for controlling rocking motion through prestressing is the ability of the cable to elongate sufficiently in order that the rocking block can rock (rotate) to an extent that involves significant lifting of its centre of gravity (CG). With a conventional steel tendon, the amount of elongation would need to be restricted to within the yield limit of about 0.002–0.004. The amount of lifting of the CG would only be 35–70 mm for a 17 m tall structure. This modest amount of lifting falls short of achieving a high enough gain of potential energy to enhance the seismic performance of a structure. In contrast, a tendon made of NiTi alloy is able to elongate by up to 10% with full recovery potential. Consider an assemblage of tendons comprising the NiTi alloy segment which is connected in series to a steel tendon segment. If only a quarter of the length of the tendon is made of the alloy, the amount of lifting can be increased to about 400 mm. The yield strength of the alloy tendon can be set below that of the steel tendon in order to keep the steel tendon responding within the elastic limit. Another important feature of the alloy is its ability to fully recover post-yield deformation, and to dissipate energy when subject to cyclic stress reversals, noting the flag shaped hysteresis behaviour of the alloy as shown in Figure 2.

The tendon assemblage as described is referred herein as the superelastic tendon. The multiple merits of the NiTi alloy as described make the superelastic tendon fit for purposes in performing the function of controlling the rocking motion in seismic conditions. The fitting of the tendon into the model of a rocking block is depicted in the schematic diagram of Figure 3.

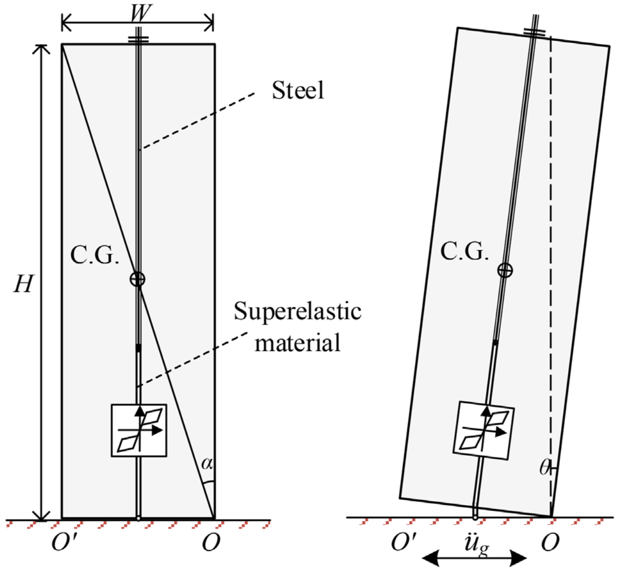


**FIGURE 3** Proposed rocking control strategy by superelastic tendon

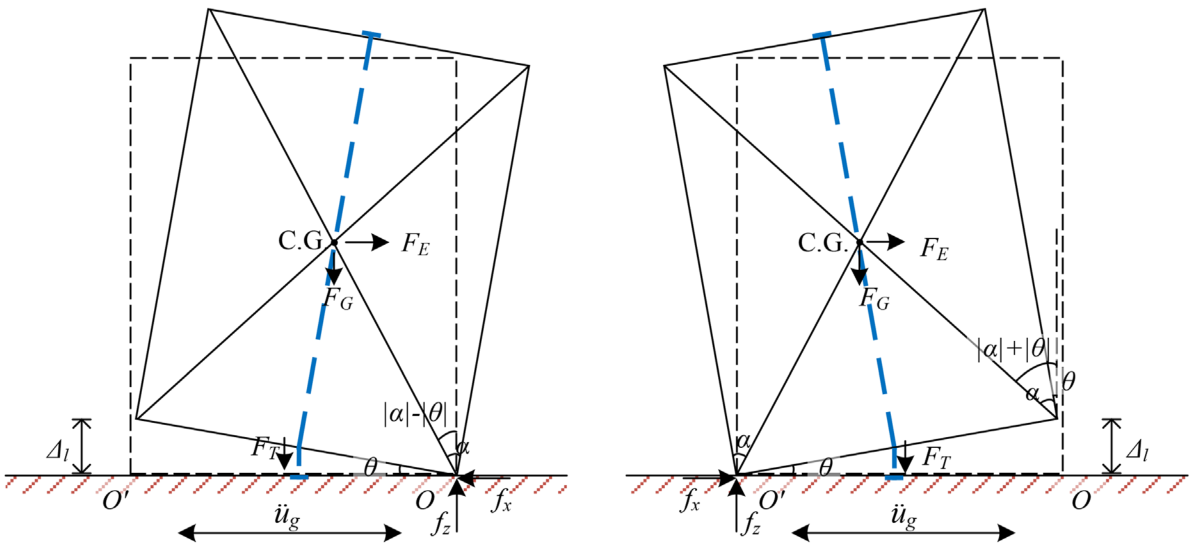


**FIGURE 4** Rigid block rocking with superelastic restraint

## 2.2 | Analytical modelling of rocking response

The objective of this section is to derive a computational algorithm for the prediction of the rotational time-history of the system which is designed to rock as a rigid rectangular block. The block is designed to rock about the pivot points $O$ and $O$' on the ground when subject to the concurrent action of the gravitational force ($F_G$), the tendon force ($F_T$) and the inertia force ($F_E$, which depends on the earthquake excitation, $\ddot{u}_g$) as shown in Figure 4. The governing equations of the system can be derived by considering the moment equilibrium about one of the pivot points.

When $\theta > 0$,

$$I_O\ddot{\theta} + F_G \cdot R\sin(\alpha - \theta) + F_T \cdot R\sin(\alpha) + F_E \cdot R\cos\ (\alpha - \theta) = 0 \tag{1}$$

When $\theta < 0$,

$$I_{O'}\ddot{\theta} + F_G \cdot R\sin(-\alpha - \theta) - F_T \cdot R\sin(\alpha) + F_E \cdot R\cos\ (-\alpha - \theta) = 0 \tag{2}$$

in which
$I_O$ and $I_{O'}$: the moment of inertia with respect to the pivot point. For rectangle block, $I_O = I_{O'} = \frac{4}{3}mR^2$
$m$: mass of the block
g: gravitational acceleration
$R$: half-diagonal length of the block
$\alpha$: angle of the slenderness of the rocking block, $\tan\alpha = b/h$
$\ddot{u}_g$: horizontal ground acceleration
$\theta$: whole-body rotation of the rigid block
$F_G$: gravitational force, $F_G = mg$
$F_T$: tendon force
$F_E$: inertia force, $F_E = m\ddot{u}_g$
Let

$$p^2 = \frac{3g}{4R} \tag{3}$$

where $p$ is a frequency parameter of the rectangular rigid block, and is expressed in the unit of rad/s. By using the sign function $sgn(\theta)$, Equations (1) and (2) can be expressed in a compact form as follows:

$$\frac{\ddot{\theta}}{p^2} = -\sin[\alpha \cdot sgn(\theta) - \theta] - \frac{F_T \cdot sin(\alpha) \cdot sgn(\theta)}{mg} - \frac{\ddot{u}_g \cdot cos[\alpha \cdot sgn(\theta) - \theta]}{g} \tag{4}$$

As the rigid block returns to the upright position, the angular velocity changes abruptly. The velocity of the block immediately following the pounding of the base on the floor is controlled by the Coefficient of Restitution (COR). In Housner's model,[8] when the pivot point for rocking shifts from $O$ to $O$', the following expression can be written as per the principles of the conservation of angular momentum:

$$I_0\dot{\theta}_1 - m\dot{\theta}_1 R\ \sin(\alpha)\cdot 2b = I_0\,\dot{\theta}_2 \tag{5}$$

in which
$b$: half of the width of the block, $b = 0.5W$
$\dot{\theta}_1$ and $\dot{\theta}_2$: the angular velocity before and after the pounding
Equation (5) can be written into Equation (6)

$$\frac{\dot{\theta}_2}{\dot{\theta}_1} = 1 - \frac{2mbR\sin(\alpha)}{I_0} = 1 - \frac{3bsin(\alpha)}{2R} \tag{6}$$

where

$$COR = \frac{\dot{\theta}_2}{\dot{\theta}_1} = 1 - \frac{3}{2}sin^2\alpha \tag{7}$$

The $COR$ can be determined experimentally by the use of Equation (8), in which $\dot{\theta}_{\mathrm{i}}$ and $\dot{\theta}_{\mathrm{i+1}}$ are the angular velocity before and after the $i$th pounding

$$COR = \frac{\dot{\theta}_{\mathrm{i+1}}}{\dot{\theta}_i} \tag{8}$$

The presented governing equations can be expressed in the vector format: $q = [\theta, \dot{\theta}]$. The first derivative of $q$ with respect to time, $\dot{q}$, can be written as $\dot{q} = [\dot{\theta}, \ddot{\theta}]$. Governing equations of the second order would then become first order differential equations, which allows the solution to be found using the ODE tools in Matlab.

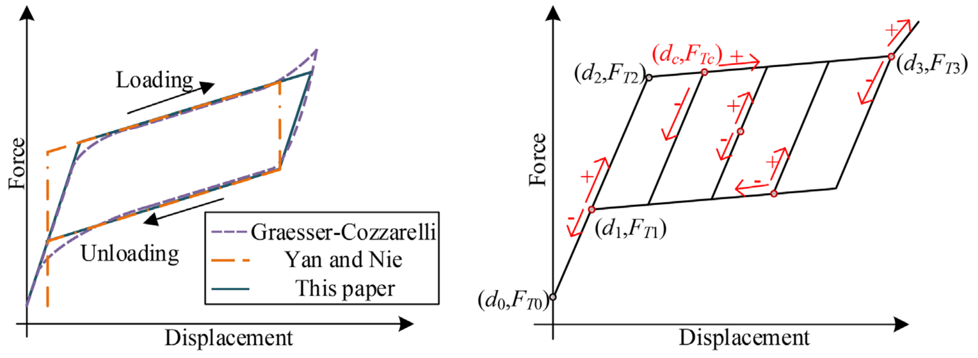


(A) Alternative hysteresis models

(B) Force-displacement ($F_T$-$d$) behaviour when subject to cyclic stress reversals

**FIGURE 5** Proposed model of force-displacement relationships of the superelastic tendon

### 2.3 | Modelling rocking response constrained by a superelastic tendon

The influence of the tendon forces on the rocking behaviour of the block as represented by the $F_T$ term in Equations (1) and (2) is well illustrated in Figure 4. This section deals with the modelling of $F_T$ in time-history analyses. The cyclic stress-strain behaviour of the superelastic tendon was originally presented by Graesser-Cozzarelli[44,45] in the form of differential equations. The force-displacement function was simplified by Yan and Nie[46] to expedite the use of the derived relationship in a time-step integration procedure. Superposing the two sets of relationships reveals discrepancies, and hence, an improved model is adopted in this study. Discrepancies of the improved model with the one as derived originally by Graesser-Cozzarelli are shown to have been much reduced. The comparison of the three force-displacement relationships is presented in Figure 5A. The model proposed in this study can be represented algebraically by Equation (9)

$$F_T(t) = f\left[d(t), d_c, F_{Tc}, sgn\left(\dot{d}(t)\right)\right] \tag{9}$$

where $d_c$ and $F_{Tc}$ are the ordinates associated with the last corner point in the hysteretic path of the tendon, and $sgn(\dot{d}(t))$is the direction of velocity at the current time step. The hysteresis model presented in the form of a force-displacement ($F_T$-$d$) diagram featuring loading and unloading as defined by the algebraic functions is presented in the schematic diagram of Figure 5B. The presented relationship was employed to define the $F_T$ term in the time-history simulation.

As a demonstration of the analytical model derived in this study, a rocking block which was 17.5 m tall and 3.5 m wide was displaced initially by applying a single ground pulse as shown in Figure 6A, resulting in a rocking response when no further ground shaking was applied. The resulting rotational behaviour of the two models in the course of the response is presented in Figure 6B, in which, separate lines represent the response behaviour of a model experiencing free rocking when unrestrained and that restrained by a prestressing superelastic tendon. The prestress force, $F_0$, was 0.5 $G$, and the first and second yielding force of the superelastic tendon, $F_1$ and $F_2$, were 0.9 $G$ and 1.6 $G$, respectively. The two energy dissipation mechanisms that have been incorporated into the modelling were: (1) energy dissipation by pounding at the base of the tower as in the case of a free rocking model, and (2) energy dissipation occurring within the superelastic tendon in the course of cyclic stress reversals. The block model experiencing free rocking was subject to the first mechanism only, whereas the restrained model was subject to both mechanisms. Time histories showing the rate of energy dissipation of the two models are presented in Figure 6C and D, respectively. The higher rate of energy dissipation of the restrained model was evident in the comparison of the time-histories simulated for the two models.

## 3 | DYNAMIC TESTING OF SCALED-DOWN MODEL

### 3.1 | General arrangement of test setup

The physical experimentation was aimed at emulating the dynamic behaviour of a (prototype) structure which was 17.5 m tall, with plan dimensions of 3.5 m by 4.2 m, and weighing 85 t. The test specimen was scaled down as a rigid block model for

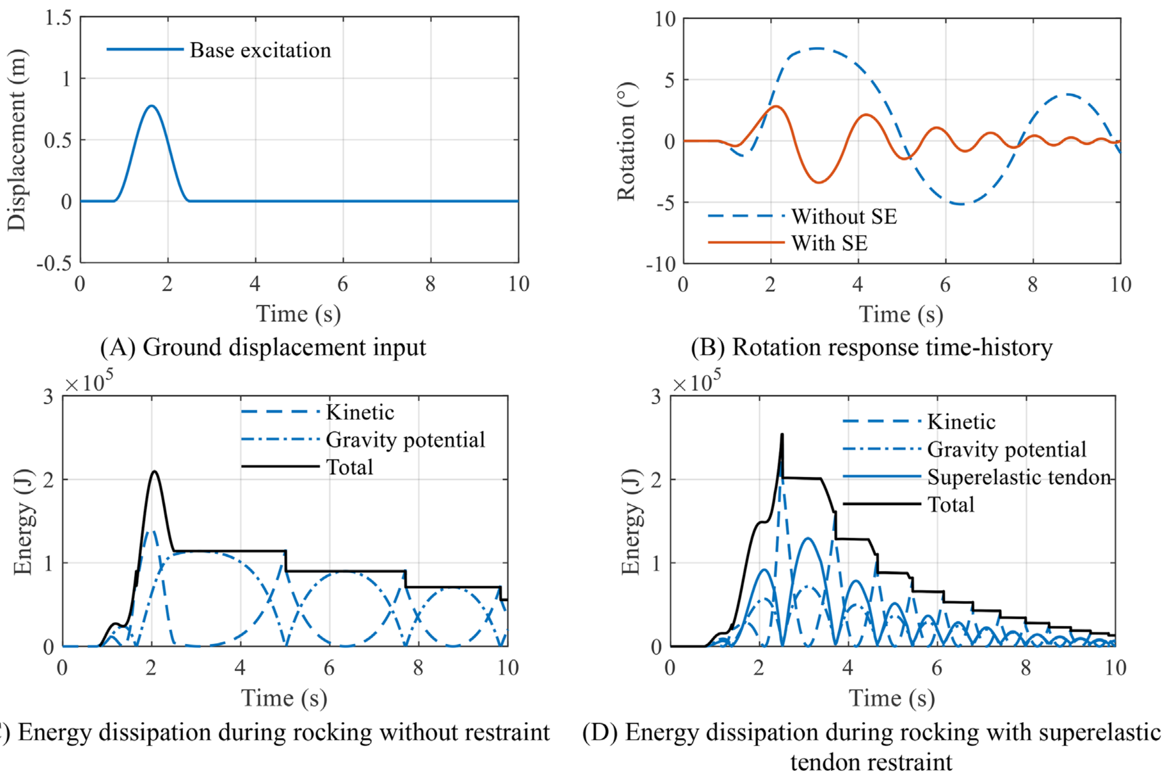


**FIGURE 6** Rocking behaviour without and with the restraint of a superelastic tendon

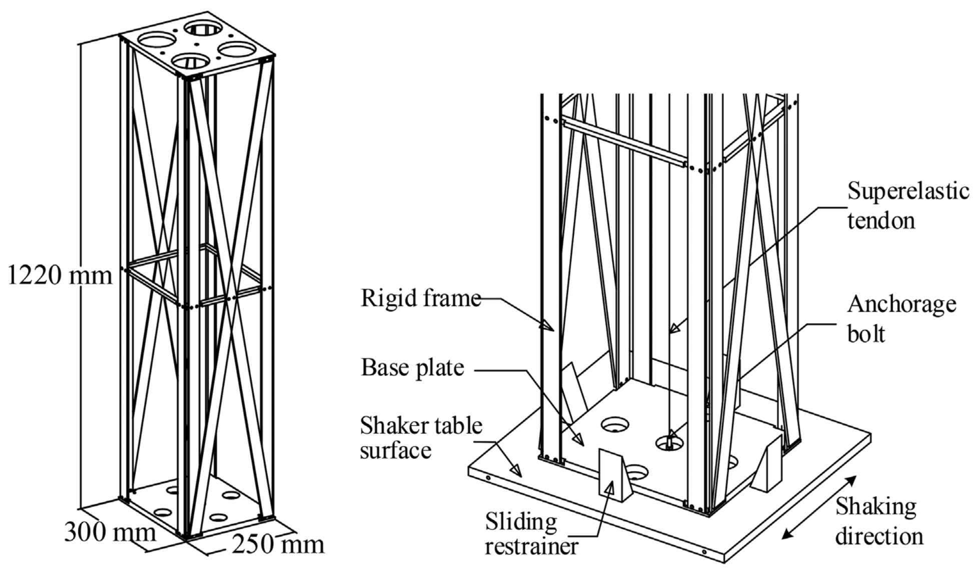


**FIGURE 7** Test specimen (left) and setup (right)

dynamic testing. The length scale was chosen as 1:14.5. Vertical acceleration was kept at 1 g (the gravitational acceleration). According to similitude laws, the scaling ratio for mass was 1:3049, and the scaling ratio for time was 1:3.8. The scaled-down model was accordingly 1.22 m tall weighing 28 kg, which conformed closely to the targeted scaling factors calculated from the similitude relationship. Refer to Figure 7 which contains the 3D perspective views of the model including the centrally positioned prestressing tendon. Also shown in Figure 7 are restrainers for preventing sliding motion in every direction and the surface of the shaker table for applying the base excitations. The prestressing tendon, which extended the full height of the model, was anchored at the shaker table surface at one end and the top plate of the specimen at

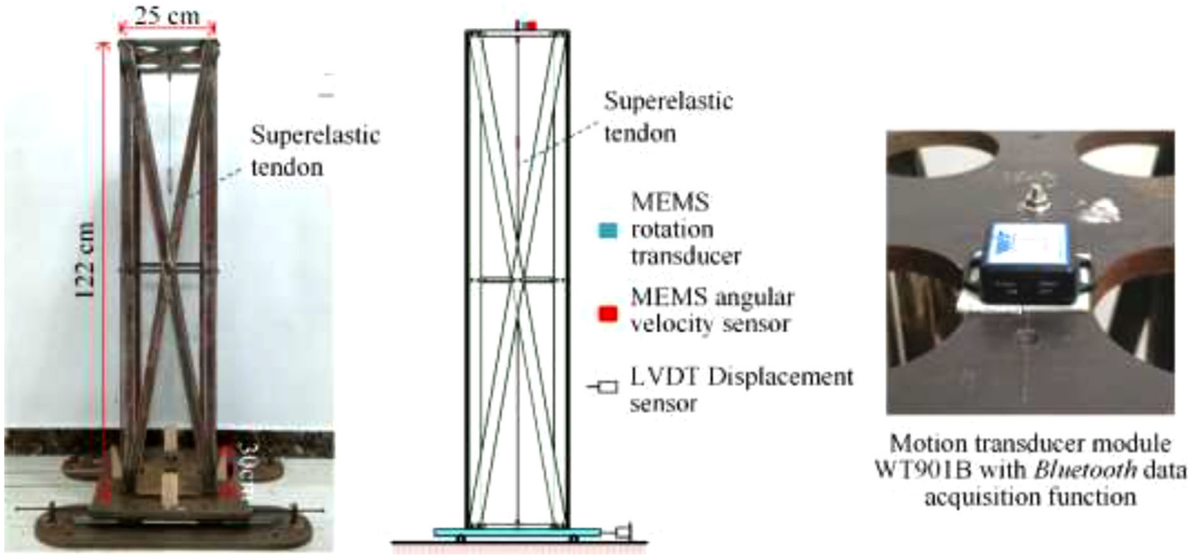


**FIGURE 8** Instrumentation setup

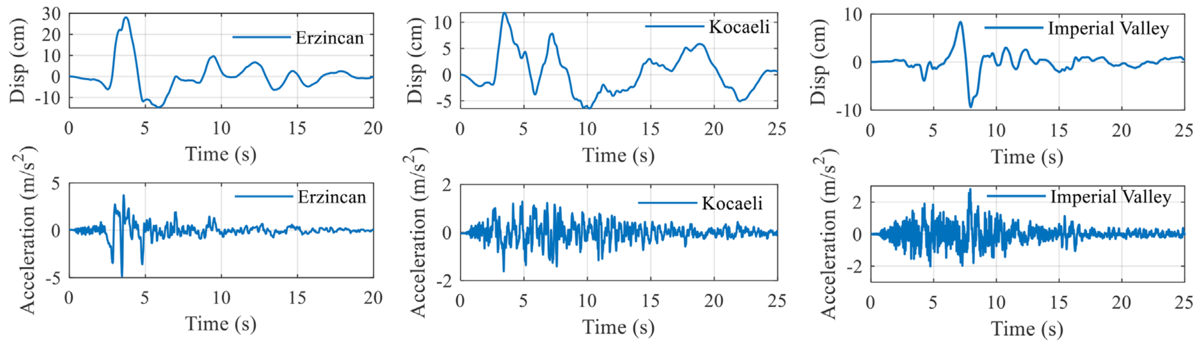


**FIGURE 9** Displacement and acceleration time-histories of example strong ground motions featuring (I) single pulse (left), (II) double pulses of the same direction (middle), and (III) double pulses of reverse directions (right)

the other end. Columns positioned at each of the corners were fully braced to achieve rigid behaviour of the model when excited into rocking motion.

A LVDT displacement transducer was used to monitor displacement of the model at the base along the direction of excitation. A micro-electro-mechanical system (MEMS) motion transducer (commonly used in robotics), weighing only about 20 g, was placed at the top of the model for measuring rotation as well as angular velocity in three orthogonal directions. Data collected from the transducers were transmitted to the computer via a *Bluetooth* data acquisition device which had an output rate of 200 Hz. A diagram along with photos showing the test setup completed with the instrumentation as described are presented in Figure 8.

## 3.2 | Test schedule

Free release tests and base excitation tests were both conducted on the model. In the free release tests, the model was initially displaced at the top to result in whole-body rotation in the vertical plane about the pivot point with an angle of $0.7\alpha$ where $\alpha$ was the critical angle that would result in overturning. The displaced model was then released and allowed to rock.

With dynamic tests involving excitations applied at the base of the scaled-down model, the excitation time-histories were derived from observations of ground displacement time-histories of several selected near-fault strong motion records[47] as shown in Figure 9. The ground displacement pulses that were employed for testing had been idealised. The idealised

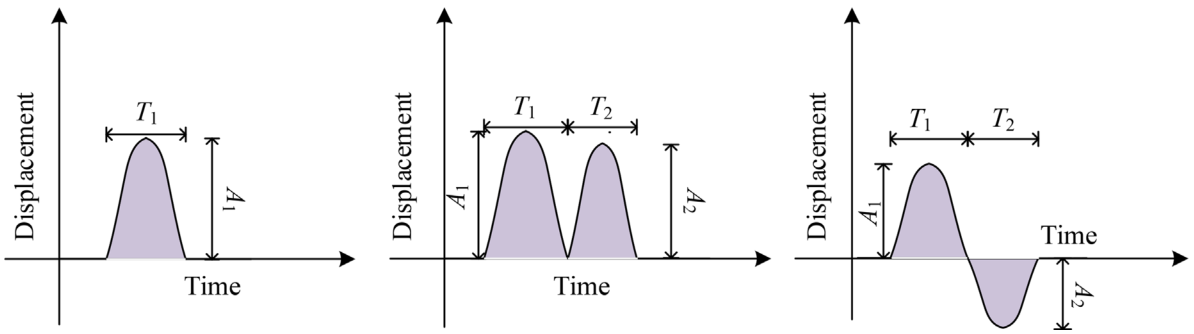


**FIGURE 10** Idealised impulses applied in base excitation tests: (I) single pulse, (II) double pulses of the same direction, and (III) double pulses of reverse directions

**TABLE 1** Test schedule

| No. | Type of test | Specimen specifications | | Excitation specifications | | | | |
|---|---|---|---|---|---|---|---|---|
| | | Restraint | Prestress | Type | $A_1$(mm) | $A_2$(mm) | $T_1$(s) | $T_2$(s) |
| 1 | Free release | No restraint | N.A. | N.A. | / | / | / | / |
| 2 | Free release | Superelastic tendon | 0.1 *G* | N.A. | / | / | / | / |
| 3 | Free release | Superelastic tendon | 0.3 *G* | N.A. | / | / | / | / |
| 4 | Base excitations | No restraint | N.A. | Pulse Type I | 63 | / | 0.55 | / |
| 5 | Base excitations | No restraint | N.A. | Pulse Type I | 102 | / | 0.63 | / |
| 6 | Base excitations | Superelastic tendon | 0.6–0.8 *G* | Pulse Type I | 77 | / | 0.51 | / |
| 7 | Base excitations | Superelastic tendon | 0.6–0.8 *G* | Pulse Type I | 103 | / | 0.66 | / |
| 8 | Base excitations | Superelastic tendon | 0.6–0.8 *G* | Pulse Type II | 75 | 60 | 0.62 | 0.65 |
| 9 | Base excitations | Superelastic tendon | 0.6–0.8 *G* | Pulse Type III | 55 | 62 | 0.48 | 0.43 |
| 10 | Base excitations | Steel tendon restraint | 0.6–0.8 *G* | Multiple Pulses Type I | 72 | / | 0.79 | / |

**G* is the weight of the specimen.

ground pulses were of three types: (I) single pulse, (II) double pulses of the same direction, and (III) double pulses of reverse directions, as shown in Figure 10. The minor trailing motions as observed on the records were not incorporated into the testing, as their inclusion was assumed to have no major bearings on the final outcome of the dynamic response of the model. Furthermore, detailed features of a recorded ground motion would not be repeated exactly in a future earthquake event. The amplitudes of the applied base excitations were adjusted to different levels for some test cases in order that the sensitivity of the rocking behaviour to changes in the intensity of ground shaking could also be studied. The period of the impulse was chosen based on consideration of the similitude relationship of time.

Different levels of prestressing were applied. Separate tests have also been conducted on the model without the restraint of the superelastic tendon. Details of the type of the test, the nature of the base excitations and the condition of the tendon restraint are summarised in the test schedule of Table 1.

## 3.3 | Static testing of superelastic tendon

The prestressing tendon of the test specimen as described in Section 3.1 comprised a single ($n = 1$) 750 mm long NiTi alloy wire of 1 mm in diameter (with a chemical composition of 55.75% Ni, 44.2% Ti and 0.05% impurities), which was connected in series to a pair ($n = 2$) of 300 mm long steel wire in 1.2 mm diameter. The elevation view of the setup of the tendon and photos of the stainless steel connectors used at different levels are shown in Figure 11.

Three identical NiTi alloy wire specimens of the same composition in 0.8 mm diameter were subject to loading-unloading tensile testing. In the static testing of the superelastic tendon, the loading protocol was displacement controlled featuring the application of three cycles of excursions. The tensile strain of the specimen was increased from 5% to 7.5% before loading to failure. This protocol was designed for obtaining the key hysteretic parameters and the ultimate strength

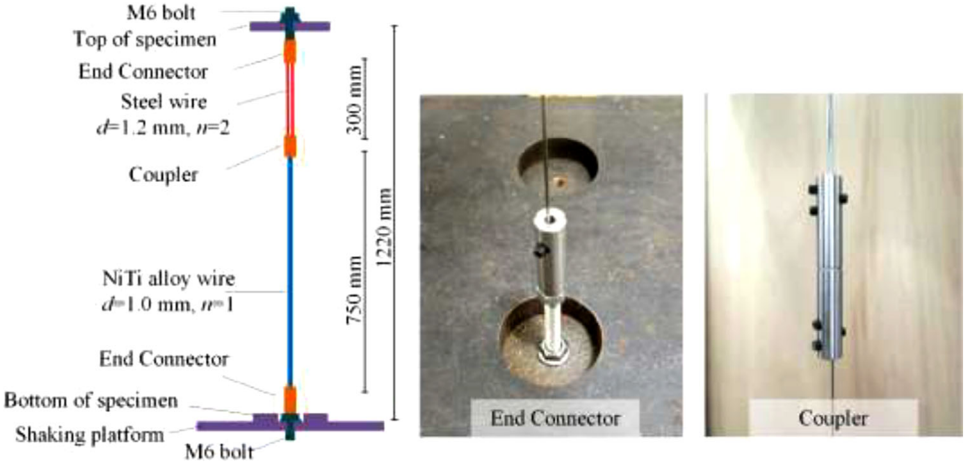


**FIGURE 11** Superelastic tendon connected in series to steel wire for rocking control

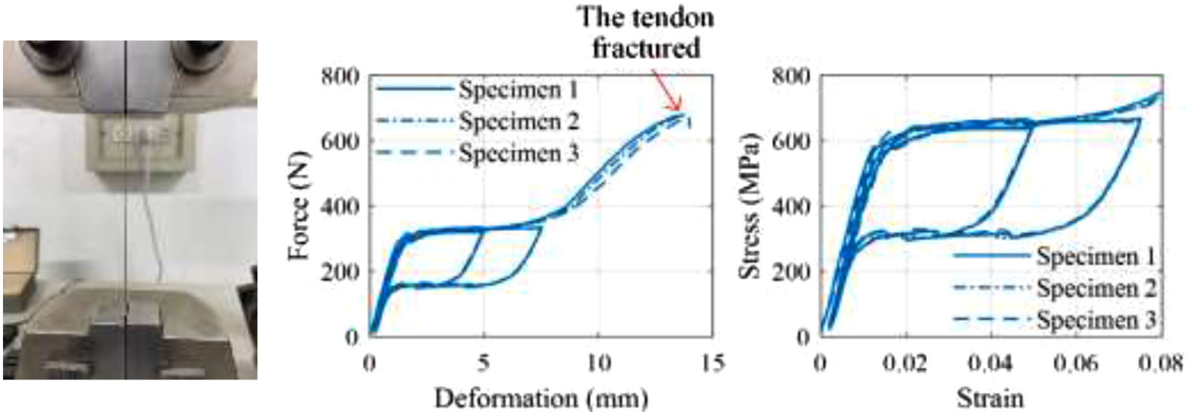


**FIGURE 12** Static testing of Nickel-Titanium (NiTi) alloy: test setup and results

of the test tendon. Other details of the testing protocol were in accordance with standard ISO 6892-1.[48] A photo showing the test setup and graphs showing the test results in the force–deformation and stress–strain formats are shown in Figure 12. The characteristic flag shaped hysteresis of the wire when subject to cyclic stress reversals was well demonstrated by static testing.

## 4 | Testing Results Analysis

The free release test #1 in Table 1 was conducted on the free-standing specimen without constraint, and test #2 and #3 were conducted on the superelastic tendon constrained specimen in two levels of prestressing: 0.1 $G$ and 0.3 $G$, where $G$ was the weight of the specimen model. The decay in the amplitude of rocking over time can be explained by the dissipation of energy through repetitive pounding of the model at the base. An important observation was the increase in the rate of diminution of the amplitude of rocking with increasing level of prestress. The diminution behaviour as described and the gradual change in the period of rocking with time have both been simulated with good accuracy by the analytical model presented in Section 2 (refer Figures 13 and 14). With tests #4–#7, similar trends in relation to the behaviour of the model experiencing free rocking response following the application of a single ground pulse (Type I) of different amplitudes can be observed with the base excitation tests, except for one case where the intensity of shaking resulted in the overturning of the free-standing model (refer Figures 15 and 16).

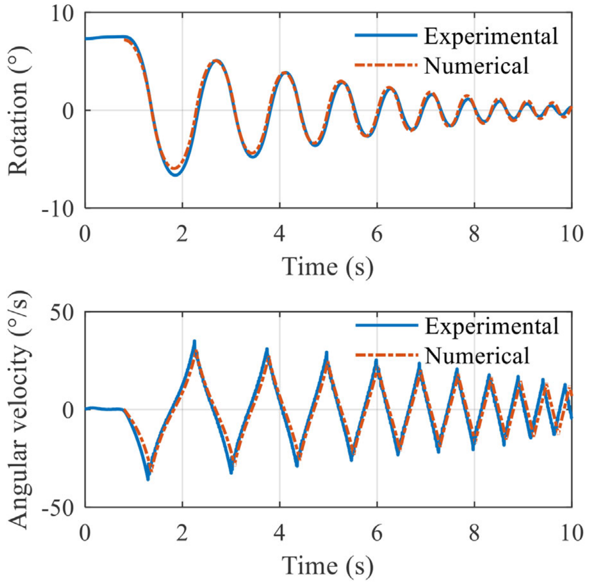


**FIGURE 13** Free release rocking response without restraints

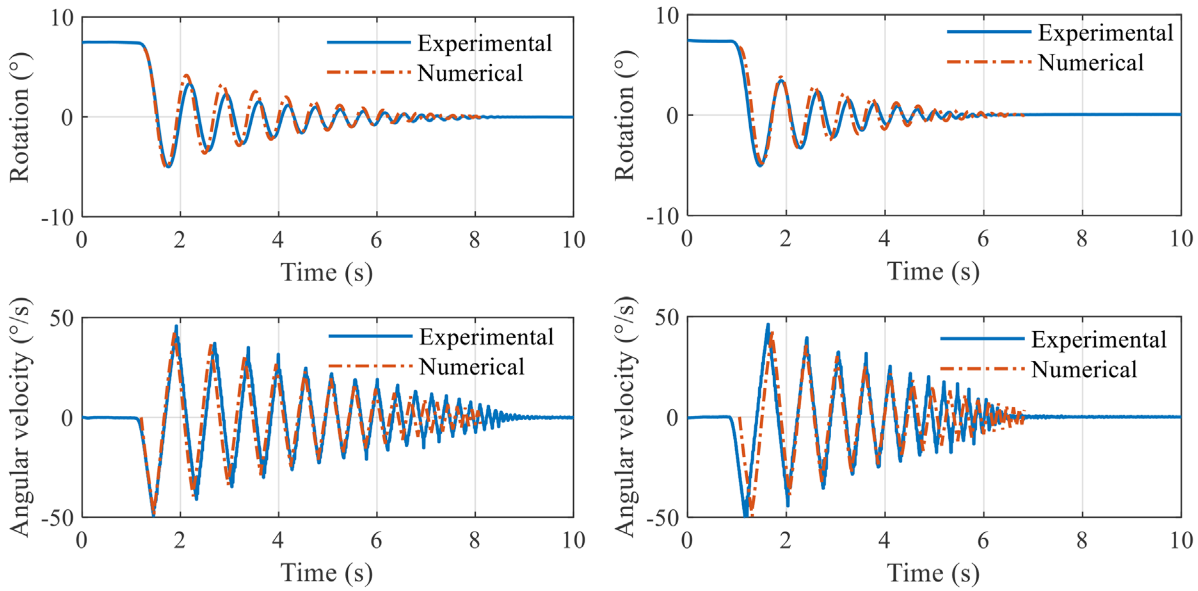


**FIGURE 14** Free release rocking response with superelastic tendon restraints: 0.1 *G* prestress (left) and 0.3 *G* prestress (right)

Further tests (#8–#9) were conducted with the application of double pulses (Type II and III). It is shown that changing the sign of the second pulse resulted in a slightly larger amount of rotation of the model when the pulse amplitude was almost the same (refer to Figure 17). With all the considered test cases, a very good match between results from numerical simulations and experimental testings have been achieved.

In the test (#10) where the prestressing tendon was a steel tendon, single pulses (Type I) of around the same amplitude were applied repetitively at intervals of around 6 seconds (Figure 18). A phenomenon of gradual increase in the rotation at the instance immediately following the pulse was observed. This observation was unique to this test. In contrast, the superelastic tendon was repeatedly used in several tests and was able to recover every time. This observation can be interpreted as the result of the accumulation of unrecoverable post-yield elongation of the steel tendon. As the tendon became slackened the prestressing action was rendered ineffective. This explanation has been confirmed by the inspection of the

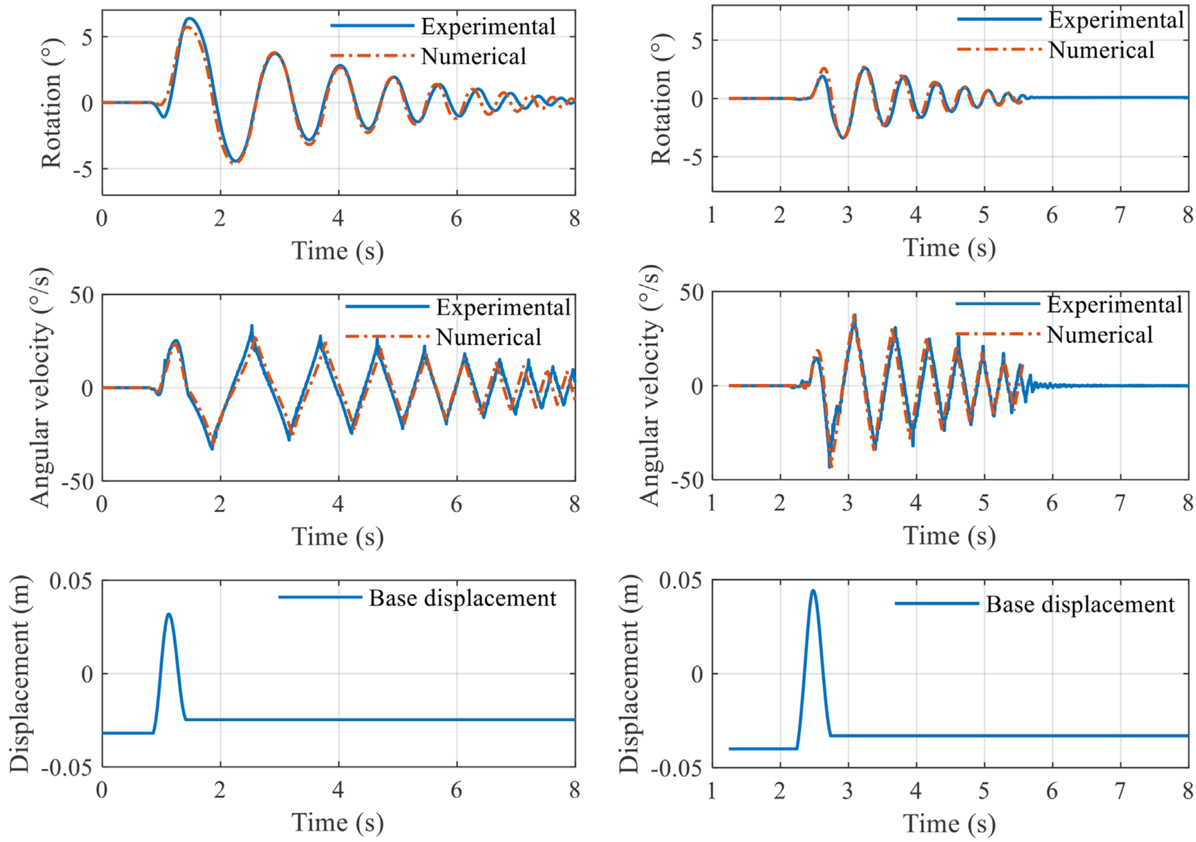


**FIGURE 15** Low-amplitude Type I pulse excited rocking response: without restraints (left) and with superelastic restraint (right)

cable following tests employing a steel tendon in comparison with observations on the superelastic tendon (refer to photos shown in Figure 19).

## 5 | Case study by numerical simulations

Results of the validation study based on dynamic testing of the scaled-down models in Section 4 give confidence in the use of the analytical model (presented in Sections 2.2 and 2.3) for macro-level seismic performance assessment of a rocking block which has the protection of a superelastic tendon. This section aims at demonstrating by case studies the application of the analytical model when applied to a prototype model of a slender tank which has incorporated the protection of the proposed innovative system. The general arrangement of the slender tank showing the principal dimensions and the layout of the key elements is shown in Figure 20. An important design parameter is the required length of the NiTi alloy segment which has the ability to fully recover elongation of up to about 10% of its length. At the limit of overturning (when the centre of gravity of the model is vertically above the pivot point), the upper end of the cable would be lifted by about 0.3 m. The cable was then designed to have the capacity to elongate by about 0.6 m (based on applying a factor of safety of 2). Given the allowable tensile strain of 10%, the minimum length of the NiTi alloy segment of the tendon was accordingly 6 m. With the case study structure, the segment length was 6.7 m which was about one-third of the total length of the entire tendon. The amount of prestressing was set at $0.25G$, and the first and second yielding force of the superelastic tendon, $F_1$ and $F_2$, were $0.55G$ and $1.0G$, respectively.

The superior performance of the case study structure which had the protection of the superelastic tendon over the control model of an unrestrained structure is well demonstrated by results from two time-history analyses which employed accelerograms recorded from the earthquake at *Erzincan* and *Kocaeli* (2.75 and 3.15 times scaling of the original wave in Figure 9 respectively), as seen in Figures 21A and B. With the *Erzincan* case study, the superelastic tendon avoided overturning which would have occurred had the rocking motion not been restrained. With the *Kocaeli* case study, the use of the superelastic tendon resulted in reducing the rotational demand by about 55%. The force-deformation behaviour

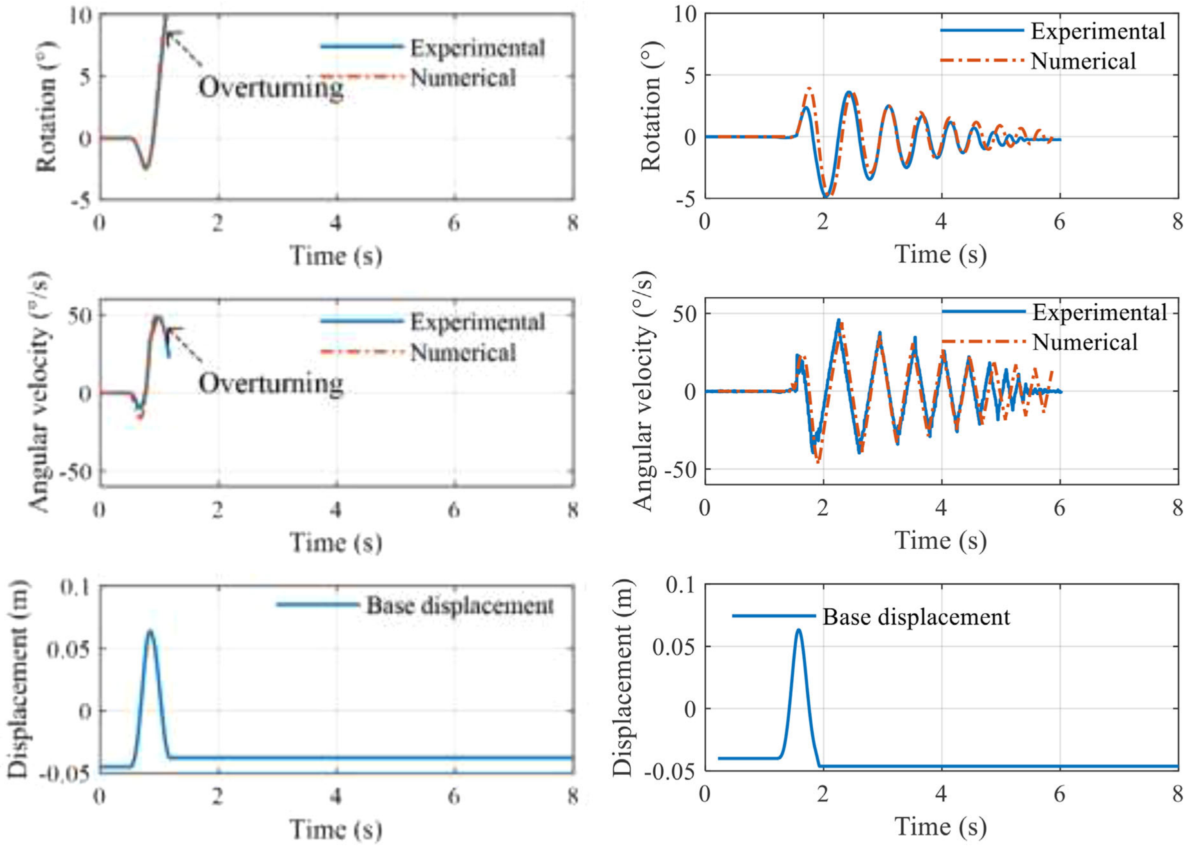


**FIGURE 16** High-amplitude Type I pulse excited rocking response: without restraints (left) and with superelastic restraint (right)

of the tendon associated with the *Erzincan* earthquake is shown in Figure 22. The loops in the force-deformation curve of the tendon in Figure 22 correspond to the major rocking cycles in time history response, which demonstrate that the superelastic tendon has yielded and recovered for multiple times during the response.

Choosing an appropriate intensity measure (*IM*) for rocking analysis is important for seismic design purposes.[49–52] Hence, it is necessary to investigate the appropriateness of various *IM* for the analysis of superelastic tendon constrained rocking structures. A parametric study employing 30 strong motions recorded from earthquake events (obtained from the PEER strong ground motion database[47]) was conducted. In the selection of the earthquake records, only near-fault station records were chosen, as the rocking structure is more sensitive to pulse-like excitations (refer to Table 2 for the listing of the accelerograms in the ensemble). The ground motions were scaled in amplitude so that most of the peak ground accelerations (*PGA*) distributed in the range of 4 $m/s^2$–15 $m/s^2$. Earthquakes within this range can occur in many areas around the globe. Earthquakes smaller than that will not initiate considerable rocking of the structure, which is out of the scope of this study.

The peak ground acceleration (*PGA*), the response spectral acceleration and the duration of strong ground shaking are the key parameters used for characterising the applied base excitations to a structure in seismic conditions. Correlations between these parameters and the response of the tendon-constrained rocking structure were examined in this study. As shown in Figure 23, both the *PGA* and the Peak Acceleration Demand (*PAD*), which is defined herein as the highest ordinate on the acceleration response spectrum for 5% damping, have been found to have no significant bearing on the rocking response. The insensitivity of the rocking response of the structure to changes in the acceleration of the base motion was observed in the study. In view of no sign of any correlations of the results shown in the graph (positioned last in Figure 23), the duration of strong ground shaking was also found not to have any systematic influence on the rocking response of the structure when the *PGAs* of all the input motions were set at the same level.

Figure 24 shows the correlations between the peak displacement demand (*PDD*), which is the highest ordinate on the displacement response spectrum for 5% damping in the natural period range of up to 5 s,[53] and the amount of rotation response. The graphs shown in the figure covered designs of nine different structural properties associated with the structure heights and conditions of the restraint. It was shown that the correlation of the rotational demand of the

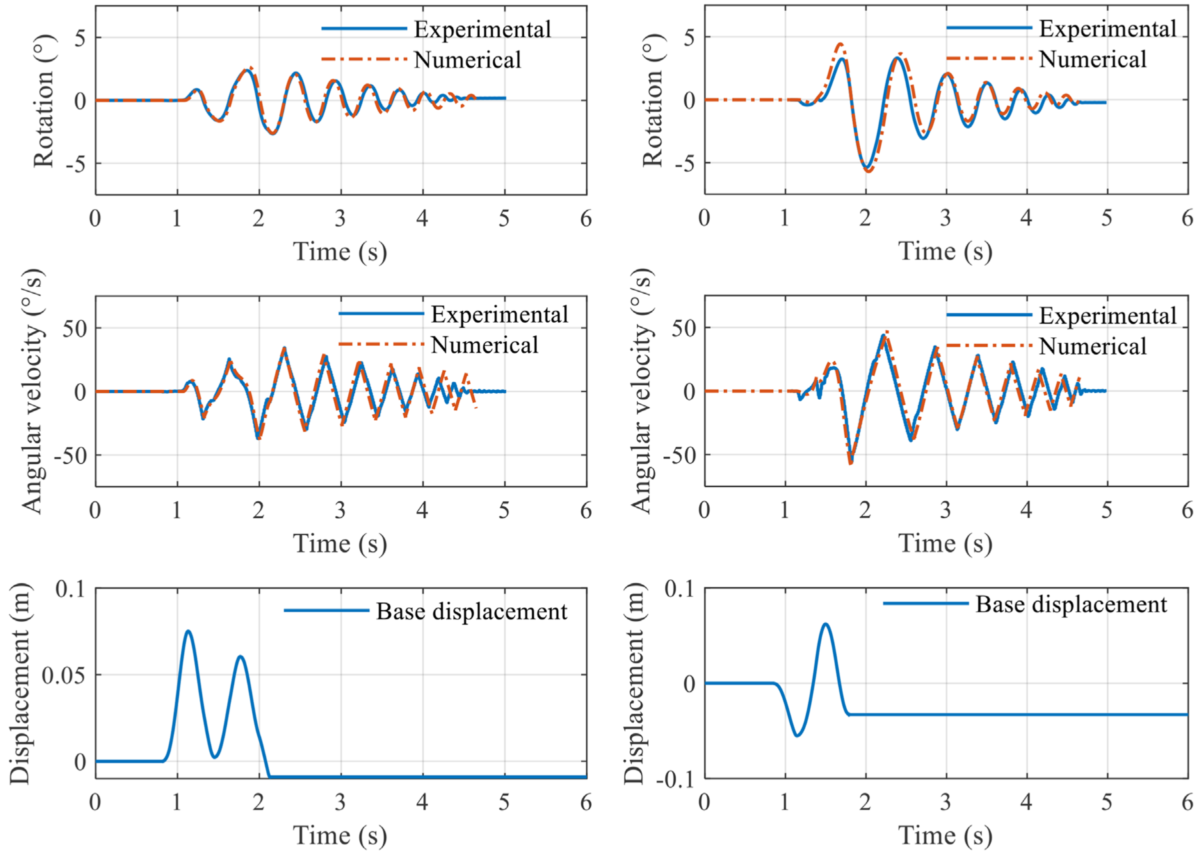


**FIGURE 17** Pulse excited rocking response with superelastic restraint: Type II pulse (left) and Type III pulse (right)

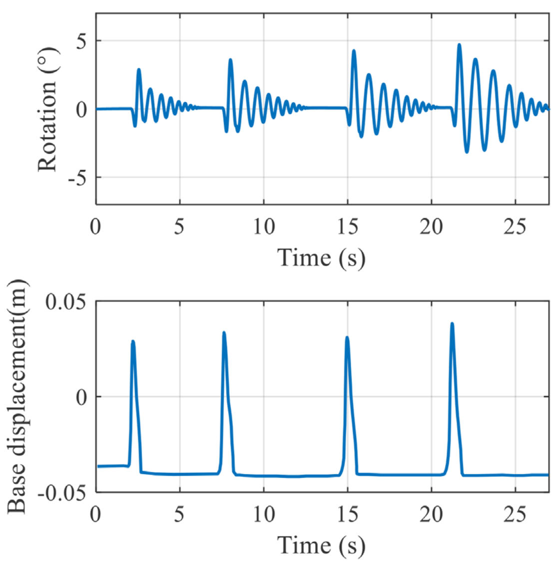


**FIGURE 18** Multiple pulses excited rocking response with steel tendon restraint

structure with the *PDD* of the base motion had a much higher coefficient of determination (*r* value) than that of the *PGA*, *PAD* or duration of ground shaking. In summary, the rotational demand of rocking with and without the restraint provided by the superelastic tendon has been made predictable by the introduction of the analytical model presented in this article.

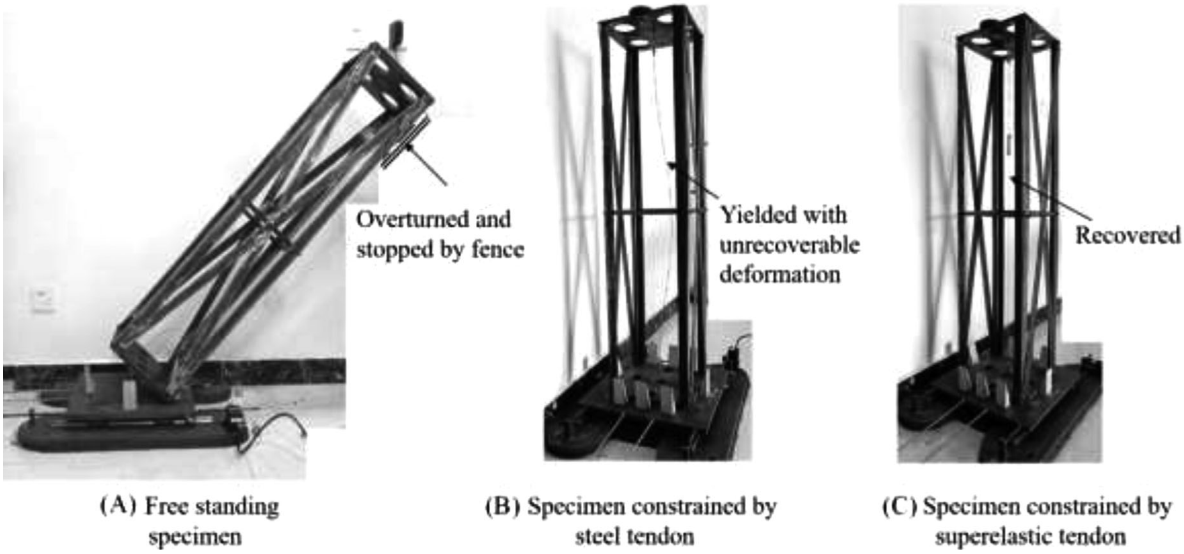


**FIGURE 19** The conditions of the specimens after testing

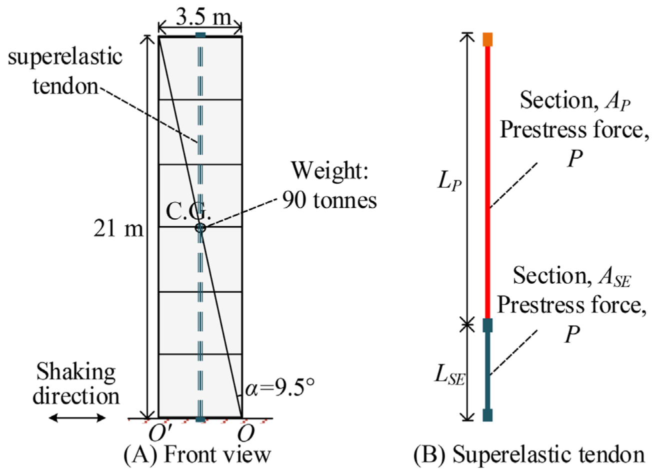


**FIGURE 20** Prototype model adopted in the numerical case study

In the simulation model and the experimental setup presented in the article, the structure is assumed to be founded on a rigid base. With a real structure, there can be a significant amount of deformation of the soil resulting from the interaction between the rocking structure and the foundation.[54] There is scope for further developing the presented model to incorporate deformation and energy dissipation occurring at the rocking interface. An important attribute of the proposed system is to make use of the rocking motion to absorb energy for relieving the strength demand on individual elements within the structure, and yet some residual energy would need to be absorbed within the structure. Thus, further studies are warranted to estimate the strength demand on individual structural elements to fulfil damage control requirements.

## 6 | Conclusions

This article introduces an innovative system for enhancing the seismic performance of structures that can be facilitated to experience large rotational (rocking) motion as a whole body. The use of superelastic tendons, which is made of the superelastic wire being connected in series with the steel wire, to restrain the rocking motion is a key feature of the proposed innovation. An important beneficial feature of a superelastic tendon over a steel tendon is the ability of the tendon to fully recover large post-elastic elongation, and to dissipate energy when subject to cyclic stress reversals.

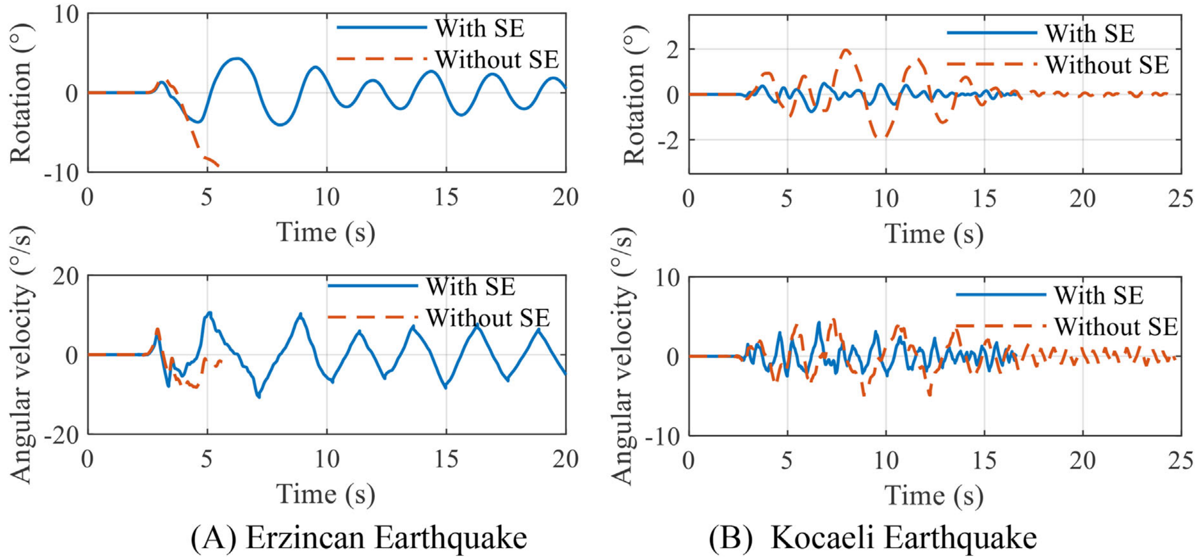


**FIGURE 21** Time histories of rocking response when subject to excitations of a recorded accelerogram. The 'SE' represents 'superelastic tendon' in the figure legend

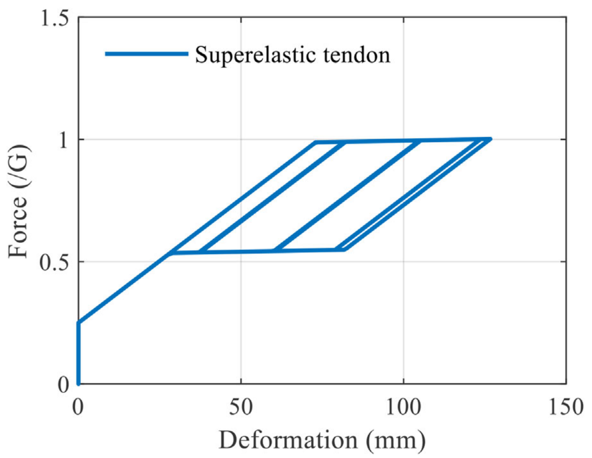


**FIGURE 22** Force-deformation relationship of the superelastic tendon under Erzincan Earthquake

The computer algorithm for generating the time-history of the rotational motion of the rocking block which has incorporated the innovative protective feature is derived from first principles.

Dynamic testing of a scaled-down model of rocking block incorporating the proposed protective mechanism has been undertaken to demonstrate the superior performance of the innovative design and to validate the accuracy of the analytical model. Case studies utilising the validated analytical model manage to reveal important trends in relation to the rotational behaviour of the structure. The rotational demand of the structure has been found to best correlate with the peak displacement demand (*PDD*) of the earthquake ground shaking. The seismic response behaviour of a rocking block which has incorporated the proposed innovative protective system is made predictable.

The development of a partially restrained rocking system for improving the seismic resistant capacity of a structure is the major achievement of this study. The effective mitigation of the seismic response behaviour of the structure, which has incorporated the use of superelastic tendons as partial restraints, is attributed to the excellent energy absorption and period elongation properties. The superelastic tendon restraint serves to reduce the risk of overturning whilst facilitating whole-body rocking to take place. The proposed system has the potential to substantially improve the capacity of the structure to counter intense seismic actions without sustaining damage.

**TABLE 2** Input near-fault ground motion records used in the numerical study

| Record sequence number | Earthquake name | Year | Magnitude | Rrup (km) | Vs30 (m/s) | 5–95% duration (s) | Scale factor |
|---|---|---|---|---|---|---|---|
| 6 | Imperial Valley-02 | 1940 | 6.95 | 6.09 | 213 | 24.2 | 2 |
| 77 | San Fernando | 1971 | 6.61 | 1.81 | 2016 | 7.3 | 2 |
| 139 | Tabas_ Iran | 1978 | 7.35 | 13.94 | 472 | 11.3 | 3 |
| 143 | Tabas_ Iran | 1978 | 7.35 | 2.05 | 767 | 16.5 | 3 |
| 170 | Imperial Valley-06 | 1979 | 6.53 | 7.31 | 192 | 13.2 | 3 |
| 171 | Imperial Valley-06 | 1979 | 6.53 | 0.07 | 265 | 8.2 | 3 |
| 183 | Imperial Valley-06 | 1979 | 6.53 | 3.86 | 206 | 6.8 | 2.75 |
| 184 | Imperial Valley-06 | 1979 | 6.53 | 5.09 | 202 | 7 | 3 |
| 313 | Corinth_ Greece | 1981 | 6.6 | 10.27 | 361 | 15.4 | 2.5 |
| 723 | Superstition Hills-02 | 1987 | 6.54 | 0.95 | 349 | 11 | 2.5 |
| 725 | Superstition Hills-02 | 1987 | 6.54 | 11.16 | 317 | 13.7 | 2.5 |
| 764 | Loma Prieta | 1989 | 6.93 | 10.97 | 309 | 13.1 | 2.5 |
| 765 | Loma Prieta | 1989 | 6.93 | 9.64 | 1428 | 6.5 | 3.15 |
| 767 | Loma Prieta | 1989 | 6.93 | 12.82 | 350 | 11.4 | 2.5 |
| 779 | Loma Prieta | 1989 | 6.93 | 3.88 | 595 | 10.2 | 2 |
| 801 | Loma Prieta | 1989 | 6.93 | 14.69 | 672 | 10.1 | 2.5 |
| 803 | Loma Prieta | 1989 | 6.93 | 9.31 | 348 | 11.1 | 1.75 |
| 821 | Erzican_ Turkey | 1992 | 6.69 | 4.38 | 352 | 8.4 | 2.75 |
| 828 | Cape Mendocino | 1992 | 7.01 | 8.18 | 422 | 17.7 | 2 |
| 1045 | Northridge-01 | 1994 | 6.69 | 5.48 | 286 | 8.8 | 1.75 |
| 1050 | Northridge-01 | 1994 | 6.69 | 7.01 | 2016 | 4.3 | 2.75 |
| 1084 | Northridge-01 | 1994 | 6.69 | 5.35 | 251 | 15.1 | 2.5 |
| 1106 | Kobe_ Japan | 1995 | 6.9 | 0.96 | 312 | 9.5 | 1.75 |
| 1111 | Kobe_ Japan | 1995 | 6.9 | 7.08 | 609 | 11.2 | 2 |
| 1114 | Kobe_ Japan | 1995 | 6.9 | 3.31 | 198 | 11.5 | 2 |
| 1120 | Kobe_ Japan | 1995 | 6.9 | 1.47 | 256 | 11.3 | 2.75 |
| 1165 | Kocaeli_ Turkey | 1999 | 7.51 | 7.21 | 811 | 15.1 | 3.15 |
| 3744 | Cape Mendocino | 1992 | 7.01 | 12.24 | 566 | 13.4 | 2.5 |
| 4876 | Chuetsu-oki_ Japan | 2007 | 6.8 | 12.63 | 655 | 11.2 | 2.25 |
| 6911 | Darfield_ New Zealand | 2010 | 7 | 7.29 | 326 | 9.5 | 2 |

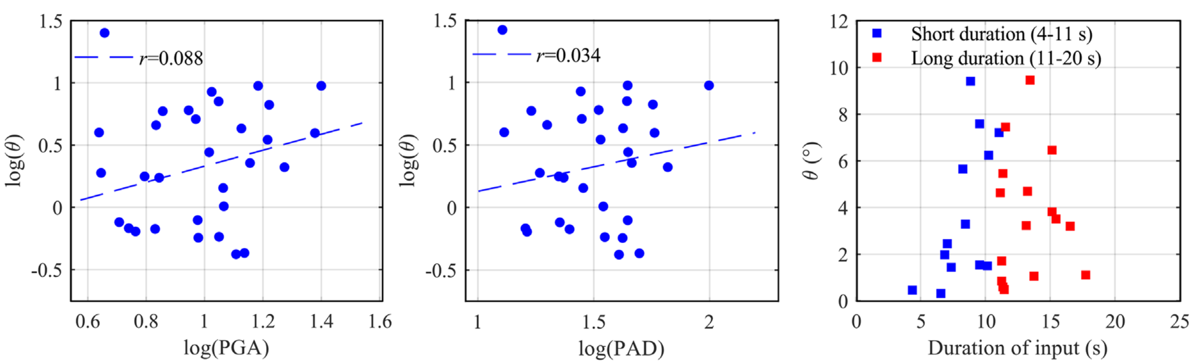


**FIGURE 23** Correlation of rocking rotation with PGA($m/s^2$) and PAD($m/s^2$) and influence of duration of ground shaking

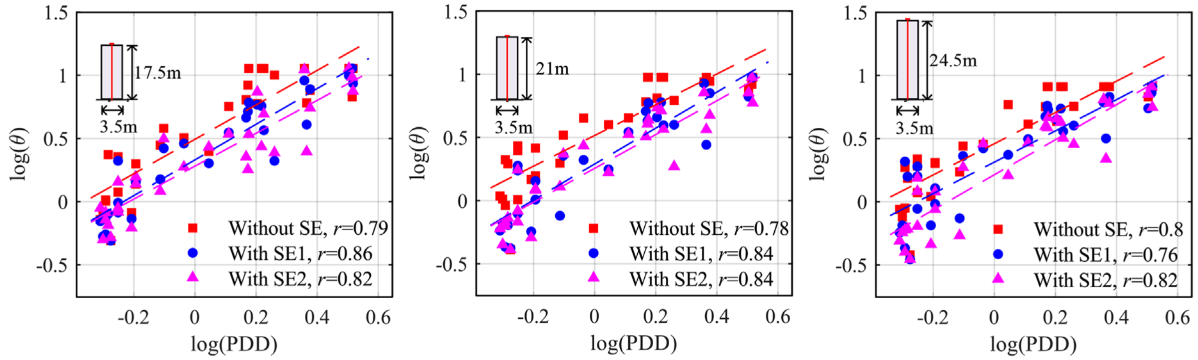


**FIGURE 24** Correlation between rocking rotation and *PDD* (m) of input excitation for structures with different configurations. In the figure legend: 'SE' denotes 'superelastic tendon restraint', 'Without SE' denotes no restraint, whereas 'SE1' and 'SE2' denote restraint with prestressing forces of 0.25 *G* and 0.5 *G*, respectively

## ACKNOWLEDGEMENTS

This work was supported by the Melbourne Research Scholarship. Open access publishing facilitated by The University of Melbourne, as part of the Wiley - The University of Melbourne agreement via the Council of Australian University Librarians.

## DATA AVAILABILITY STATEMENT

The data that support the findings of this study are available from the corresponding author upon reasonable request.

## ORCID

*Sheng Li* https://orcid.org/0000-0001-8739-2171
*Hing-Ho Tsang* https://orcid.org/0000-0002-4912-5184

## REFERENCES

1. Kurama YC. Seismic design of unbonded post-tensioned precast concrete walls with supplemental viscous damping. *ACI Struct J*. 2000;97(4):648-658.
2. Makris N, Aghagholizadeh M. The dynamics of an elastic structure coupled with a rocking wall. *Earthquake Eng Struct Dyn*. 2017;46(6):945-962.
3. Kurama Y, Pessiki S, Sause R, Lu LW. Seismic behavior and design of unbonded post-tensioned precast concrete walls. *PCI Jl*. 1999;44(3):72-89.
4. Mpampatsikos V, Egidio M, Belleri A, Nascimbene R. A non-dimensional parametric approach for the design of PT tendons and mild steel dissipaters in precast rocking walls. *Eng Struct*. 2020;212:110513.
5. Wang B, Han Q, Jia Z, Du X. Seismic response analysis of the precast double-deck rocking frame bridge pier system. *Soil Dyn Earthquake Eng*. 2021;146:106745.
6. Makris N, Vassiliou MF. Planar rocking response and stability analysis of an array of free-standing columns capped with a freely supported rigid beam. *Earthquake Engng Struct Dyn*. 2013;42:431-449.
7. Pollino M, Bruneau M. Dynamic seismic response of controlled rocking bridge steel-truss piers. *Eng Struct*. 2008;30:1667-1676.
8. Housner GW. The behavior of inverted pendulum structures during earthquakes. *Bull Seismol Soc Am*. 1963;53(2):403-417. https://doi.org/10.1785/bssa0530020403.
9. Priestley MJN, Evison RJ, Carr AJ. Seismic response of structures free to rock on their foundations. *Bull N Z Natl Soc Earthquake Eng*. 1978;11(3):141-150.
10. Ishiyama Y. Motions of rigid bodies and criteria for overturning by earthquake excitations. *Earthquake Eng Struct Dyn*. 1982;10:635-650.
11. Makris N, Zhang J. Rocking Response and Overturning of Anchored Equipment Under Seismic Excitations. PEER Report 1999/06; 1999.
12. Makris N & Black C Rocking Response of Equipment Anchored to a Base Foundation. PEER Report 2001/14; 2001.
13. Muhinadeen MMM Collapse Behaviour of Prefabricated Modular Buildings Under Seismic Conditions. The University of Melbourne (PhD Thesis); 2020.
14. Aslam M, Godden WG, Scalise DT. *Earthquake Rocking Response of Rigid Bodies*. Lawrence Berkeley National Laboratory; 1978(LBL-7983).
15. Midorikawa M, Azuhata T, Ishihara T, Wada A. Seismic response analyses of rocking structural systems with yielding base plates by the finite element method. *WIT Trans Built Environ*. 2005;81:333-341.
16. Han Q, Jia Z, Xu K, Zhou Y, Du X. Hysteretic behavior investigation of self-centering double-column rocking piers for seismic resilience. *Eng Struct*. 2019;188:218-232. https://doi.org/10.1016/j.engstruct.2019.03.024.

17. Aghagholizadeh M. A finite element model for seismic response analysis of vertically-damped rocking-columns. *Eng Struct*. 2020;219:110894. https://doi.org/10.1016/j.engstruct.2020.110894.
18. Aghagholizadeh M, Makris N. Response analysis of yielding structures coupled to rocking walls with supplemental damping. *Earthquake Eng Struct Dyn*. 2021;50(10):2672-2689. https://doi.org/10.1002/eqe.3466.
19. Amin M, Yang TY, Bagatini-cachuço F, Pan S. Seismic design and performance evaluation of controlled rocking dual-fused bridge system. *Eng Struct*. 2020;212:110467. https://doi.org/10.1016/j.engstruct.2020.110467.
20. Thiers-Moggia R, Málaga-Chuquitaype C. Performance-based seismic design and assessment of rocking timber buildings equipped with inerters. *Eng Struct*. 2021;248:113164. https://doi.org/10.1016/j.engstruct.2021.113164.
21. Thiers-Moggia R, Málaga-Chuquitaype C. Seismic protection of rocking structures with inerters. *Earthquake Eng Struct Dyn*. 2018;48:528-547. https://doi.org/10.1002/eqe.3147.
22. Makris N, Kampas G. Seismic protection of structures with supplemental rotational inertia. *J Eng Mech*. 2016;04016089:1-11.
23. Thiers-Moggia R, Málaga-Chuquitaype C. Seismic control of flexible rocking structures using inerters. *Earthquake Engng Struct Dyn*. 2020;49:1519-1538. https://doi.org/10.1002/eqe.3315.
24. Thiers-Moggia R, Málaga-Chuquitaype C. Dynamic response of post-tensioned rocking structures with inerters. *Int J Mech Sci*. 2020;187:105927. https://doi.org/10.1016/j.ijmecsci.2020.105927.
25. Dehcheshmeh EM, Broujerdian V. Determination of optimal behavior of self-centering multiple-rocking walls subjected to far-field and near-field ground motions. *J Build Eng*. 2022;45:103509. https://doi.org/10.1016/j.jobe.2021.103509.
26. Li Y, Li J, Shen Y. Quasi-static and nonlinear time-history analyses of post-tensioned bridge rocking piers with internal ED bars. *Structures*. 2021;32:1455-1468. https://doi.org/10.1016/j.istruc.2021.03.099.
27. Song G, Yang TY, Zhou Y. Performance evaluation of self-centering rocking shear walls: part 1—quantification of structural damages. *Structures*. 2021;34:2515-2529. https://doi.org/10.1016/j.istruc.2021.09.024.
28. Song G, Yang TY, Zhou Y. Performance evaluation of self-centering rocking shear walls: part 2—determination of performance objectives. *Structures*. 2021;34:3404-3413. https://doi.org/10.1016/j.istruc.2021.09.030.
29. Nazari M, Sritharan S. Influence of different damping components on dynamic response of concrete rocking walls. *Eng Struct*. 2020;212:110468. https://doi.org/10.1016/j.engstruct.2020.110468.
30. Liu Q, French CW, Sritharan S. Comparative response of rocking-wall systems with cast-in-place and precast floor systems in buildings. *Eng Struct*. 2021;234:111942. https://doi.org/10.1016/j.engstruct.2021.111942.
31. San Juan J, Nó ML. Superelasticity and shape memory at nano-scale: Size effects on the martensitic transformation. *J Alloys Compd*. 2013;577(Suppl. 1):S25-S29. https://doi.org/10.1016/j.jallcom.2011.10.110.
32. Xia J, Noguchi Y, Xu X, et al. Iron-based superelastic alloys with near-constant critical stress temperature dependence. *Science*. 2020;369(6505):855-858. https://doi.org/10.1126/science.abc1590.
33. Ozbulut OE, Hurlebaus S, Desroches R. Seismic response control using shape memory alloys: a review. *J Intell Mater Syst Struct*. 2011;22(14):1531-1549. https://doi.org/10.1177/1045389%D7;11411220.
34. Qiu CX, Zhu S. Characterization of cyclic properties of superelastic monocrystalline Cu-Al-Be SMA wires for seismic applications. *Constr Build Mater*. 2014;72:219-230. https://doi.org/10.1016/j.conbuildmat.2014.08.065.
35. Fang C, Zheng Y, Chen J, Yam MCH, Wang W. Superelastic NiTi SMA cables: thermal-mechanical behavior, hysteretic modelling and seismic application. *Eng Struct*. 2019;183:533-549. https://doi.org/10.1016/j.engstruct.2019.01.049.
36. Wang B, Zhu S, Chen K, Huang J. Development of superelastic SMA angles as seismic-resistant self-centering devices. *Eng Struct*. 2020;218:110836. https://doi.org/10.1016/J.ENGSTRUCT.2020.110836.
37. Ghowsi AF, Sahoo DR. Seismic response of SMA-based self-centering buckling-restrained braced frames under near-fault ground motions. *Soil Dyn Earthquake Eng*. 2020;139: 106397. https://doi.org/10.1016/j.soildyn.2020.106397.
38. Chen J, Fang C, Wang W, Liu Y. Variable-friction self-centering energy-dissipation braces (VF-SCEDBs) with NiTi SMA cables for seismic resilience. *J Constr Steel Res*. 2020;175:106318. https://doi.org/10.1016/j.jcsr.2020.106318.
39. Gur S, Mishra SK, Chakraborty S. Stochastic optimization of shape-memory-alloy rubber bearing (SMARB) for isolating buildings against random earthquake. *Struct Control Health Monit*. 2014(21):1222-1239. https://doi.org/10.1002/stc.
40. Gur S, Mishra SK, Chakraborty S. Performance assessment of buildings isolated by shape-memory- alloy rubber bearing: comparison with elastomeric bearing under near-fault earthquakes. *Struct Control Health Monit*. 2014;21:449-465.
41. Ma QTM. *The Mechanics of Rocking Structures Subjected to Ground Motion*. The University of Auckland (PhD Thesis); 2010.
42. Čeh N, Jelenić G, Bićanić N. Analysis of restitution in rocking of single rigid blocks. *Acta Mech*. 2018;229(11):4623-4642. https://doi.org/10.1007/s00707-018-2246-8.
43. Aslam M, Godden WG, Scalise DT. *Rocking and Overturning Response of Rigid Bodies to Earthquake Motions*. Lawrence Berkeley National Laboratory 1978(LBL-7539).
44. Graesser EJ, Cozzarelli FA. Shape-memory alloys as new materials for aseismic isolation. *J Eng Mech*. 1991;117(11):2590-2608. https://doi.org/10.1061/(asce)0733-9399(1991)117:11(2590).
45. Graesser EJ, Cozzarelli FA. A proposed three-dimensional constitutive model for shape memory alloys. *J Intell Mater Syst Struct*. 1994;5:78-89.
46. Yan X, Nie J. Response of SMA superelastic systems under random excitation. *J Sound Vib*. 2000;238(5):893-901. https://doi.org/10.1006/jsvi.2000.3020.

47. Pacific Earthquake Engineering Research Center (PEER). *PEER Ground Motion Database*. http://peer.berkeley.edu/products/strong_ground_motion_db.html.
48. International Organization for Standardization. ISO 6892-1:2016 Metallic materials—tensile testing—part 1: method of test at room temperature. 2016.
49. Bakhtiary E, Gardoni P. Probabilistic seismic demand model and fragility estimates for rocking symmetric blocks. *Eng Struct*. 2016;114:25-34. https://doi.org/10.1016/j.engstruct.2016.01.050.
50. Kavvadias IE, Vasiliadis LK, Elenas A. seismic response parametric study of ancient rocking columns. *Int J Arch Heritage*. 2017;11(6):791-804. https://doi.org/10.1080/15583058.2017.1298009.
51. Kavvadias IE, Papachatzakis GA, Bantilas KE, Vasiliadis LK, Elenas A. Rocking spectrum intensity measures for seismic assessment of rocking rigid blocks. *Soil Dyn Earthquake Eng*. 2017;101:116-124. https://doi.org/10.1016/j.soildyn.2017.07.021.
52. Reggiani Manzo N, Vassiliou MF. Displacement-based analysis and design of rocking structures. *Earthquake Eng Struct Dyn*. 2019;48(14):1613-1629.
53. Kafle B, Lam N, Gad E, Wilson J. Displacement controlled rocking behaviour of rigid objects. *Earthquake Eng Struct Dyn*. 2011;40:1653-1669.
54. Elgawady MA, Ma Q, Butterworth JW, Ingham J. Effects of interface material on the performance of free rocking blocks 2011(July 2010):375-392. https://doi.org/10.1002/eqe.1025.

**How to cite this article:** Li S, Tsang H-Ho, Lam N. Seismic protection by rocking with superelastic tendon restraint. *Earthquake Engng Struct Dyn*. 2022;51:1718–1737. https://doi.org/10.1002/eqe.3635